

Surface Morphology Analysis of graphene transfer on SiO₂ with BPA aptasensor detection using Electrochemical Impedance Spectroscopy

Nur Insyirah Ahmad Shukri¹, Norhayati Sabani^{2,3*}, Mohamad Faris Mohamad Fathil¹, Syarifah Norfaezah Sabki^{2,3}, Ruslinda A. Rahim¹, Nur Hamidah Abdul Halim¹, Nur Syakimah Ismail^{2,3}

¹ Institute of Nano Electronic Engineering, Universiti Malaysia Perlis, 01000, Kangar, Perlis Malaysia.

² Faculty of Electronic Engineering & Technology, Universiti Malaysia Perlis, 02600 Arau, Perlis, Malaysia

³ Micro System Technology, Centre of Excellence (MiCTEC), Universiti Malaysia Perlis, 02600 Arau, Perlis, Malaysia.

Received 12 Oct 2022, Revised 16 Feb 2023, Accepted 4 March 2023

ABSTRACT

Bisphenol A or BPA is one of the highest produced chemicals in the world. The production of polycarbonate plastic and epoxy resin are used to make variety of consumer goods and it is frequently employed BPA as a raw material. BPA is one of the endocrine disruptors which is related to a wide range of adverse health effects that can cause reproductive disorders and many kinds of cancers. In the work, the novelty of electrochemical sensor of BPA was constructed on a graphene modified electrode using graphene transfer method. In this work, High-power microscope and scanning electron microscopy were used to study the production and characterization of the graphene, with two significant mapping graphene at 20% and 80%. The existence of graphene on silicon oxide was analyzed using Raman Spectroscopy while the composition of the materials was analyze using Fourier-Transform Infrared Spectroscopy. In this analysis, both analysis data from Raman and FTIR clearly shown that 80% mapping graphene is the best option which resulting to the high surface coverage. The electrochemical performance of the mapping 80% graphene electrode was examined using Electrochemical Impedance Spectra. The increase in charge transfer resistance (R_{ct}) both before and after the addition of BPA denotes the development of the charge at the electrode surface. The equivalent circuit shows the R_{ct} of graphene increased from 0.4 k Ω to 1.2 k Ω and drastically increased to 300 k Ω when the device was introduced with BPA due to the existence of a negative charge carrier and the repelling contact.

Keywords: Electrochemical aptasensor, Graphene, Graphene Transfer, Aptamer, BPA

1. INTRODUCTION

Over the recent years, electrochemical biosensor is serving as solid support for immobilization of biomolecules events such as antigen-antibody interaction [1], enzyme-substrate reaction [2] and aptamer-specific molecules bind (aptasensor) [3],[4]. The aptasensor or aptamer specific molecules was selected due to small size of aptamer which allow high binding affinity [5]. Aptamer is one of the short-chain oligonucleotides of ribonucleic acid (RNA) or singles stranded deoxyribonucleic acid (DNA) that can bind strongly with the target molecule and exhibit greater affinity for target [6]. The uniqueness of aptamer has been broadly used as recognition probes by researcher including peptides [7], proteins [8], molecules [9] and even whole cells [10]. In this project, the molecule is Bisphenol A (BPA). BPA is an endocrine disrupting chemical which is widely used in industrial production that could mimic the action of hormone oestrogen and mix up estrogen receptor binding process of human, and reduce immune function [6],[11]. The use of polycarbonate plastics and epoxy resins in production such as beauty industry, children's toys,

* Corresponding author: hayatisabani@unimap.edu.my

and food industry bring negative effects on environment and human health [11]. Therefore, the development of aptasensor for BPA detection generates continuous interests.

Electrochemical sensor is a perfect instrument as it is faster, low cost and more economical to develop the detection of BPA and produce good findings in this research. The performance of the electrochemical sensors depends on the electrode material. Graphene is one of the typical nanocarbon that received much attention due to its great electrical conductivity [12], high surface area [13] and thinnest electrode material [14] which it is known as viable electrode material for electrochemical sensors [15]. Furthermore, to its special electrical properties and chemical stability, graphene is also able to resist oxidation in solution under low voltage [16]. Graphene can be synthesized using numerous techniques from simple methods to the use of advanced methods that utilize special equipment [17]. The most widely used technique for studying graphene (on a macroscale) involves drop-casting aliquots of a graphene dispersion onto a supporting electrode surface, essentially immobilising graphene [18],[19]. Nevertheless, altering such surfaces runs the risk of exposing underlying 'reactive' surfaces, which can affect and (in some circumstances) dominate the reported electrochemistry [18]. Edward *et al.* found that the solvent evaporation pushed the graphene platelets to the edges of the underlying electrode which cause capillary forces [14]. Since the method has some of the disadvantages, graphene transfer is being favoured by researchers due to their scalability, cost, and time effectiveness [20]. In this work, a graphene transfer method is used to develop the graphene electrode on silicon substrate that will be used as an electrochemical sensor to detect BPA.

2. EXPERIMENTAL METHOD

2.1 Graphene transfer

Figure 1 depicts the graphene transfer method in details. In order for the graphene electrode successfully transferred onto the silicon oxide/silicon (SiO₂/Si), it is essential to follow a few steps of graphene transfer process. Fabrication of graphene electrode began with substrate preparation, which consists of bare silicon wafer cleaning, oxidation process and graphene preparation. The first step in the graphene transfer procedure was to spin-coat graphene/nickel for 30 seconds at 1500 rpm with a thin layer of poly-methyl methacrylate (PMMA). Then, nickel-coated graphene was baked for 5 minutes at 100°C. After that, the graphene-nickel part was completely covered with a few droplets of poly-dimethyl siloxane (PDMS). The polymers were then cured for 3 minutes at 100°C until they became rigid. The next stage for transferring graphene was to etch Ni foils in iron (III) chloride (FeCl₃) for 30 minutes after the polymers had already set. A thin, semi-transparent film that floated on the solution surface was left behind after Ni was etched in FeCl₃. PMMA is utilised because it is acetone dissolvable, while PDMS serves as an adhesion booster and protective layer.

After the nickel etching as in Figure 1(a), the graphene substrate on PMMA/PDMS was cleaned in distilled water for several times, then was left on the water to be scooped using spatula as shown in Figure 1(b). Then, it is carefully placed on top of target substrate which is SiO₂ as in Figure 1(c). After that, the excess water on the substrate was wiped followed by applying gentle pressure to the top of PDMS using wooden rod to eliminate excess water and air as seen in Figure 1(d). Then the sample is transferred into the oven to be annealed for 3 minutes to ensure the samples are completely dry (Figure 1(e)). The graphene transfer may not be evenly covered if the extra water and air are not completely removed. Lastly, the sample was immersed in acetone to dissolve PMMA, which leaves graphene on SiO₂/Si as shown in Figure 1(f-g). To increase the Van der Waals force between graphene and SiO₂, the procedure was repeated by spin coating PMMA on graphene/SiO₂/Si and then re-immersing the mixture in acetone.

The surface morphology of the graphene that had been applied to the substrate was subsequently examined using high power microscope (HPM) and scanning electron microscopy (SEM). Before

the graphene testing process with aptamer immobilisation and BPA detection started, graphene on SiO₂ was first incubated in sulfuric acid to promote covalent functionalization of graphene using the destructive approach.

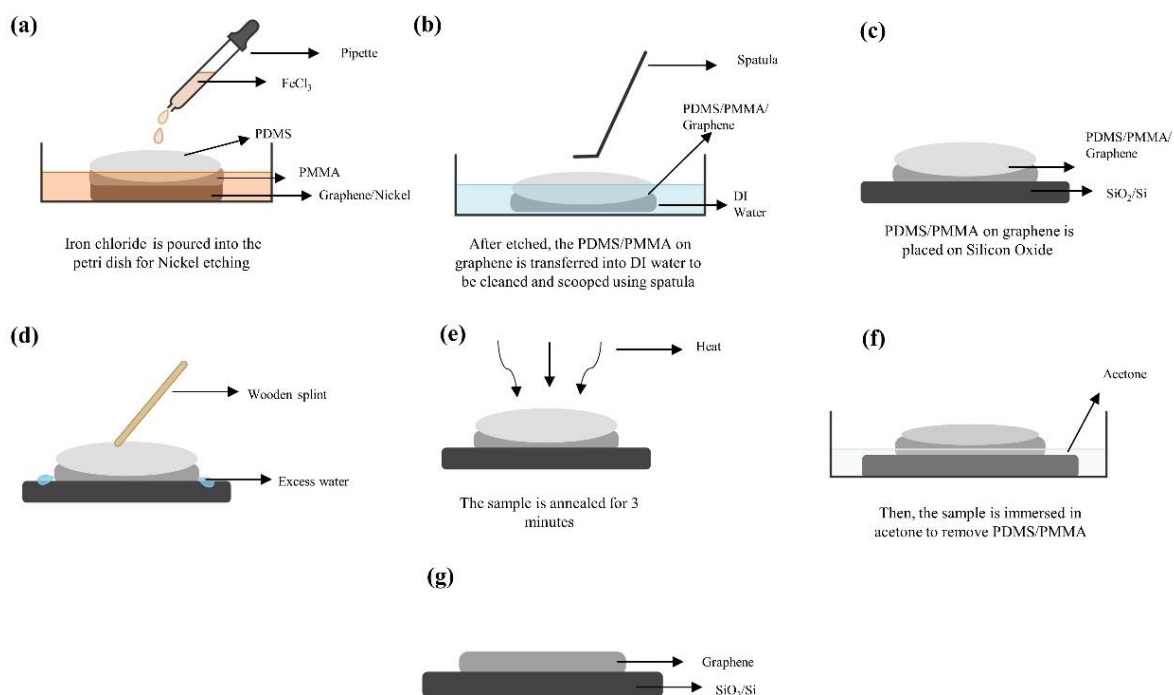


Figure 1. Process of transferring graphene (a) Ni etched in FeCl₃, leaving PDMS/PMMA/graphene behind (b) PDMS/PMMA/graphene transferred to SiO₂/Si substrate using spatula. (c) PDMS/PMMA/graphene PDMS are placed on top of a SiO₂ substrate. (d) excess water/air is removed by using wooden splint. (e) bake until it dries in furnace. (f) Graphene on SiO₂ substrate after being removed from PDMS/PMMA/graphene in acetone. (g) SiO₂ base with graphene.

2.2 Surface functionalization and detection

Figure 2 depicts the covalent functionalization of graphene using a destructive approach after it had been exposed to sulfuric acid (H₂SO₄) for a brief period of time as shown in Figure 2(b). Then, graphene surface was incubated with single-stranded oligonucleotides (Figure 2(c)). The surface functionalization started with incubating the device in mixture of N-(3-Dimethylaminopropyl)-N'-ethyl carbodiimide (EDC) and N-Hydroxysuccinimide (NHS) for amine-coupling reaction for attachment of carboxyl with aptamer. The mixture of 2 mg EDC and 2 mg NHS were dissolved in 1 mL DI water and leave it on graphene surface for 30 minutes in room temperature and later rinsed with DI water to wash away weakly bond EDC/NHS.

After that, the functionalize graphene electrode was started with incubating the device with 2 mL of 0.4 nM with sequence BPA-specific aptamer 5'AmMC6/GGG CCG TTC GAA CAC GAG CAT GCC GGT GGG TGG TCA GGT GGG ATA GCG TTC CGC GTA TGG CCC AGC GCA TCA CGG GTT CGC ACC AGG ACA GTA CTC AGG TCA TCC TAG-3' for 24 hours at room temperature. First, the aptamer was dissolved in phosphate buffer saline and diluted in serial dilution. Then, graphene electrode was placed in 10 mL beaker consist of aptamer to be incubated for 24 hours and placed in vacuum cabinet to maintain the humidity and temperature of the graphene electrode. The surface of graphene was rinsed with 50μL PBS solution and DI water to remove unbound molecules. The functionalize of aptamer on the graphene will be characterized using Fourier-Transfer Infrared Spectroscopy (FTIR) and Electrochemical Impedance Spectroscopy (EIS).

Immobilized aptamer on graphene surface is then incubated with Bisphenol A as shown in Figure 2(d). BPA with molecular weight 228 g/mol was dissolved in methanol (5 mL) with a concentration of 0.5 nM, then incubated with the aptamer/graphene electrode for 30 minutes. The graphene substrate was washed with PBS solution and DI water before each measurement to get rid of any residue and unattached molecules. The characterization of the immobilization between the aptamer and BPA was measured using Fourier-Transfer Infrared Spectroscopy (FTIR) and Electrochemical Impedance Spectroscopy (EIS). The minimum concentration of BPA that will be used in this project is 0.5 nM.

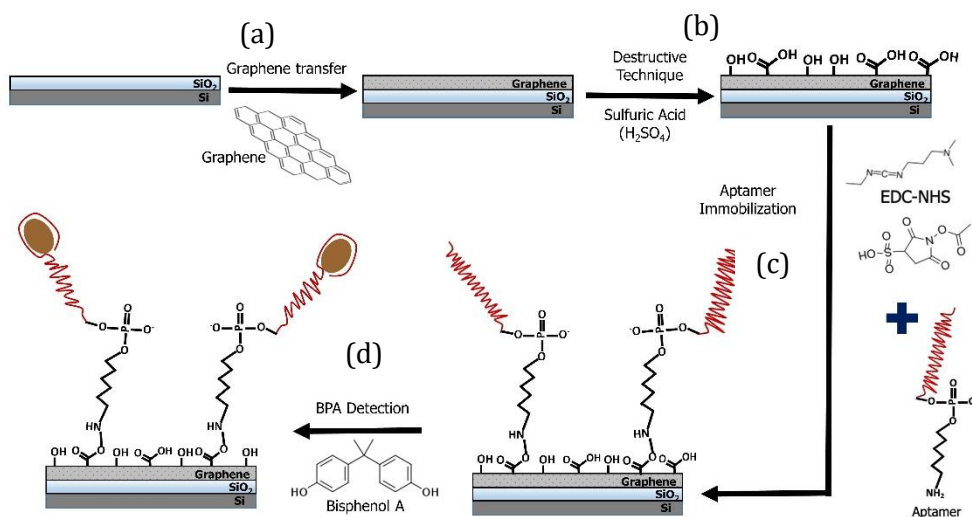


Figure 2. Overall process steps for BPA detection

3. RESULTS AND DISCUSSION

3.1 Morphology

3.1.1 Scanning electron microscope (SEM)

The fabrication of the electrode was completed using a graphene transfer method. As a result, graphene electrodes are well fabricated according to the naked eyes. The fabricated graphene electrode morphology was inspected and analysed using high power microscope (HPM) and scanning electron microscope (SEM). Figure 3 shows the image of graphene in working distance of 5 kV and 15 kV with magnification of 1000 x and 2000 x.

Based on Figures 3(a) and (b), it can be seen that graphene was successfully transferred to the SiO₂ substrate since it had a characteristic flakes-like structure. When graphene is transferred in water, some areas of the substrate may peel off and reveal some of the wrinkles even when the transfer is complete. Moreover, some undesired contaminants that may be brought on by PMMA or dusts are seen in the images. Since PMMA is non-conductive and provides scattering sites, the significant PMMA residue on the graphene may have an impact on its electrical performance and ability to transmit charges effectively [21]. From these images, graphene with 80% coverage shows better typical flakes structure compared to 20% coverage. This may be due to the graphene peel off in the water during graphene transfer from PDMS/PMMA/graphene to SiO₂. Moreover, it is crucial to make sure that any excess water or air trapped during the graphene transfer process is eliminated before the material is placed on top of the SiO₂ in order to have a superior structure.

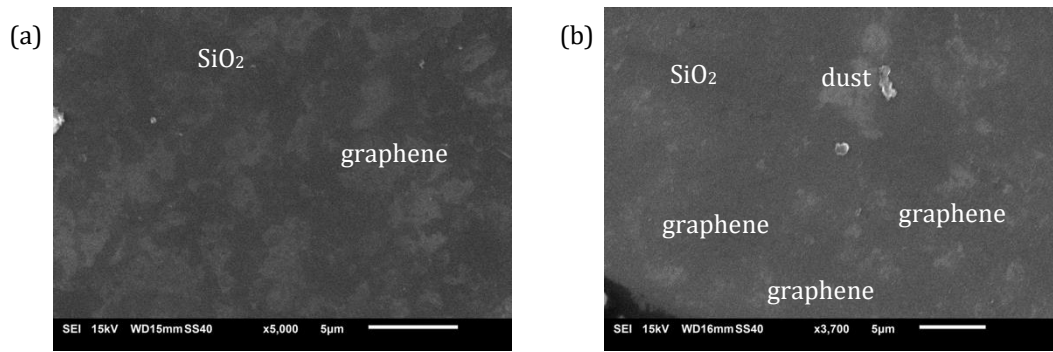
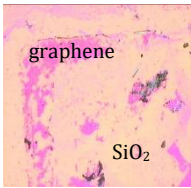
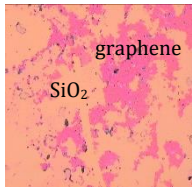
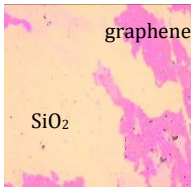
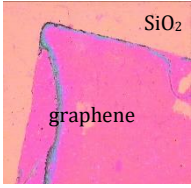
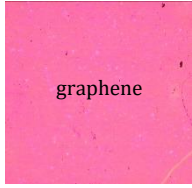



Figure 3. SEM image of (a) 20%, (b) 80%

3.1.2 High Power Microscopy

ECLIPSE L300N HPM from Nikon was used under the maximum magnification power to analyze the morphology of the graphene fabricated on Si wafer. Table 1 lists the optical images of silicon substrate with graphene layer under 10 x magnification. The results show two different sample mappings which are 20% mapping and 80% mapping. Based on observation, sample with mapping at 80% shows better active area compared to 20%. The 20% of the graphene coverage was poorly mapped because the graphene was only partially bonded to the PDMS/PMMA, which caused the graphene to peel off when the PDMS/PMMA was removed in acetone. Graphene sheets from Nickel are typically one atom thick thus cracking easily happens as a result of mechanical strain imposed during cleaning and repetitive transfer and damage from sharp tools such as tweezers [22]. Moreover, other than the peeled off the graphene, the image also shows some residue and contamination which are polymer residue and dusts that might occur during the transfer process. However, the dust impurities can be removed during immersion in acetone. The polymer residue which PMMA can be removed by lengthening the immersion time or duration of the graphene substrate in acetone.

Table 1. Image from a high-power microscope (HPM) showing the transfer of graphene on a substrate with 20% and 80% mapping

Sample (% mapping)	10x Magnification		
20	 <p>graphene SiO₂</p> <p>Above edge</p>	 <p>graphene SiO₂</p> <p>Middle</p>	 <p>graphene SiO₂</p> <p>Peel off</p>
80	 <p>SiO₂ graphene</p> <p>Above edge</p>	 <p>graphene</p> <p>Middle</p>	 <p>graphene</p> <p>Peel off</p>

3.1.3 Raman Spectroscopy

Figure 4 shows a Raman spectra of graphene transfer with 20% mapping and 80% mapping which was obtained using Confocal Micro-Raman Imaging system, Horiba/Xplora Plus instrument with wavelength of 532 nm. The Raman spectrum of graphitic materials consist of three distinct bands, which are D band, G band and 2D band as shown in Figure 4 (b). The D band, G band and 2D band for graphene transfer with 80% mapping are at 1340.24 cm⁻¹, 1578.16 cm⁻¹, and 2674.83 cm⁻¹, respectively.

In general, graphene produces two high optical peaks in Raman spectra which are the G and 2D band. Based on the Raman spectra graph for 80% mapping, the intense peak of G band (1578.16 cm⁻¹) in the graph corresponding to the first scattering of E_{2g} and higher frequency of E_{2g} phonon [23],[24]. So, it showed that the deposited material is graphite which composed with sp² bonded carbon in planar sheet. The presence of D band (1340.24 cm⁻¹) in the graph indicates the dwindle in size of the in-plane sp² during the graphite chemical oxidation [24], thus the D band attributed to disordered structure of graphite and minor defects in the graphene sheets. Other than that, the graph shows the 2D band (2674.83 cm⁻¹) due to breathing modes of the hexagonal rings of carbons atoms and this 2D band also can be used to determine the number of graphene layers [25].

Based on Figure 4 (a), it showed no Raman peak for graphene. The high optical peaks in graphene 20% mapping has shown intense peaks at value less than 1000 cm⁻¹ which indicates the enhancement factor of PMMA [26]. This also may due to the peeled off graphene which contribute to more PMMA residue on top of the SiO₂. Based on the Raman spectrum, it was shown that no graphene on the SiO₂ for the graphene with 20% mapping.

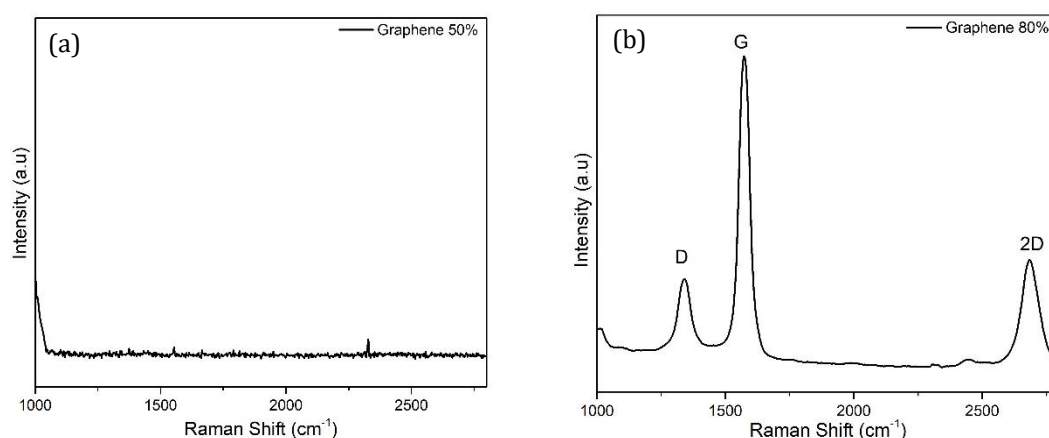


Figure 4. Raman spectroscopy of graphene. (a) Graphene with 50% mapping (b) Graphene with 80% mapping.

3.1.3 Fourier-transform infrared spectroscopy

FTIR spectra was calibrated first on graphene sample. In the FTIR spectrum of pristine graphene, it showed no significant peaks which relevant to any functional groups indicating that the functionalization steps have introduced in treated graphene, aptamer functionalize and BPA immobilization [27]. The weak bands that appear on the graph can be assigned to the absorption of water molecules, which hydrogen is attached directly to the aromatic rings in range 3000 cm⁻¹ and above. In graphene spectrum, the weak peaks can be seen in the range 1600 to 1500 cm⁻¹ appeared to be the absorption of C=C bonds stretching which corresponding to the graphene structure. Based on Figure 5 (b), graphene with mapping 80% shows the graphene properties when it was measured under FTIR.

When the graphene was treated with sulphuric acid (H_2SO_4) using the destructive method [28], the peaks appeared in the spectrum shows the exfoliated graphene due to the intercalation of some reactants implied in the process [29]. The CO groups (CO stretching vibrations) 1022.24 cm^{-1} (for graphene with 20% mapping) and 1012.88 cm^{-1} (for graphene with 80% mapping) in treated graphene indicates the prime extended conjugated π -orbital from alkoxy. Meanwhile, the C=O bond shows the appearance of carboxylic acid and carbonyl moieties at 612.58 cm^{-1} (for graphene with 80%). The last peak to be on the graph is hydroxyl (OH) out-of-plane bend which it may cause by excess water on the sample [27].

Next, a stable layer of BPA-specific aptamer which contains amino groups (NH_2) was functionalized onto the surface of treated graphene. In Figure 5 (b), an intense peak of C-N 1170.87 cm^{-1} for graphene 80% mapping was clearly appeared to be amide III for aliphatic amines which is noticeable on the FTIR spectra and represents as medium or weak band for aliphatic amines in the range of non-aromatic amines [30]. C-N stretch is considered as weak band because the peak region of C-N stronger than C-O stretch as the ionization of nitrogen is higher than oxygen [31]. Figure 5 (a) which was 20% mapping of graphene, there was no peak of C-N stretch at all.

Lastly, the intense peak from 1168.65 cm^{-1} were appeared as amide III which covalently bind between NH_2 group and BPA for graphene with 80% mapping whereas no peak was seen for graphene with 20% mapping.

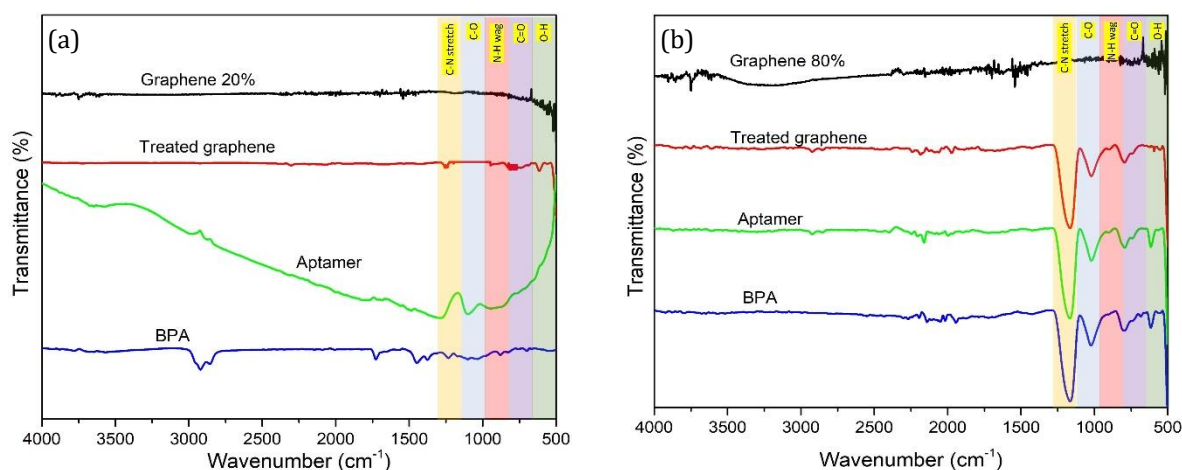


Figure 5. Graph of Fourier-transform Infrared Spectroscopy of graphene with mapping (a) 20% and (b) 80% mapping

3.1.4 Electrochemical impedance spectroscopy

In electrochemical measurement, the changing of modified interfacial layer on the electrode correspond to the change in R_{ct} values which results in changes in the intensity of electron transfer from redox species onto the electrode [32]. In this measurement the graphene aptasensor is being measured in potassium ferricyanide, $K_3[Fe(CN)_6]$ that act as redox reaction. The equivalent circuit that has been produced as shows in Figure 6 (iv). For graphene electrode, the charges on the graphene are either uncharged, negatively charged or positively charged [33]. The electron transfer from potassium ferricyanide was adhered on the graphene surface. Figure 6 (i-iii) shows the illustration of electron transfer from $K_3[Fe(CN)_6]$ to the graphene electrode.

Based on the results that have been gathered in Raman and FTIR, it shows that 80% mapping of graphene could be used to detect the BPA. In this work, it can be clearly observed that the electron-transfer resistance increases from $0.4\text{ k}\Omega$ to $300\text{ k}\Omega$ resulting in hindrance of diffusion of redox marker thus causing an increase in R_{ct} value. Figure 6 (i) shows that when graphene

electrode was being measured, the R_{ct} value of graphene electrode is in the range 0.4 k Ω indicating $K_3[Fe(CN)_6]$ went through directly to the graphene electrode and due to the absence of the resistive aptamer/BPA layer on the electrode.

After the aptamer was being immobilized on graphene electrode, the successful of aptamer immobilization resulted in increased in R_{ct} recorded at range 1.2 k Ω as in Figure 6 (ii). The negatively-charged aptamer repels the redox reaction and making the R_{ct} value increased and this prove that negatively charged aptamer enhanced the charge transfer of the graphene electrode [34].

Next, after BPA was introduced the R_{ct} value showed a drastic change with from 1.2 k Ω to 300 k Ω for graphene 80% mapping as stated in Figure 6 (iii). This result is in consideration to occur due to effectively adhere of large amount of BPA on aptamer, insulating the electrode and preventing the electrolytes from reaching the electrode surface [35].

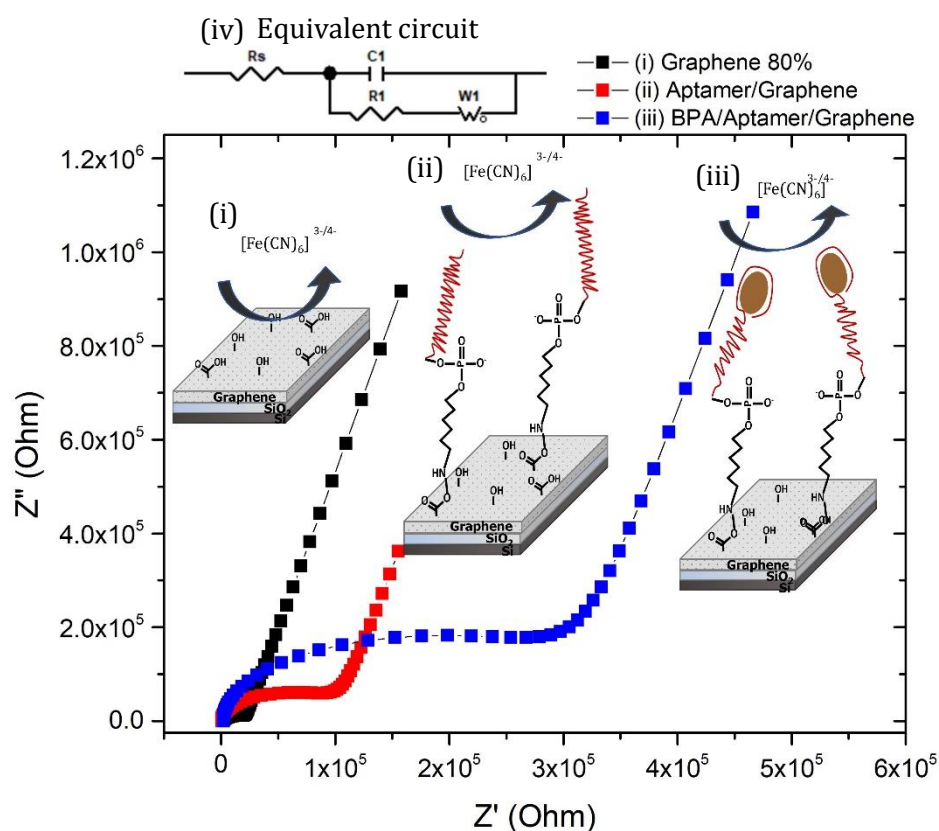


Figure 6. Schematic illustration of EIS of BPA at the aptamer-immobilized graphene electrode

4. CONCLUSION

In conclusion, it can be said that the fabrication of graphene on SiO₂ substrate was successfully transferred with mapping of 80% by using graphene transfer method. The SEM images showed that 80% mapping graphene showing the graphite structure which can be proved with Raman spectroscopy while the peeled off 20% graphene showed no graphene Raman spectrum on top of the substrate. Other than that, the FTIR showed no significant peak for 20% mapping graphene compared to the 80% mapping graphene. The BPA detection was done using 80% mapping graphene. The R_{ct} of graphene increased from 0.4 k Ω to 1.2 k Ω and was drastically increased to 300 k Ω when it was introduced with BPA. In conclusion, the presence of a negative charge carrier and the repelling contact with the electrochemical probe caused the R_{ct} to increase [3].

ACKNOWLEDGEMENTS

The inventors would like to thank the Ministry of Higher Education of Malaysia for their assistance through the Fundamental Research Grant Scheme (FRGS) under grant number FRGS/1/2018/STG07/UNIMAP/02/7. The inventors would also want to thank all of the staff at the Faculty of Electronic Engineering and Technology (FKTEN), Institute of Nano Electronic Engineering (INEE), and University Malaysia Perlis for the granted funding that makes this significant research feasible and successful.

REFERENCES

- [1] J. R. North, "Immunosensors: antibody-based biosensors," vol. 3, no. 7, pp. 180–186, 1985.
- [2] Z. Wang and Z. Dai, "Carbon nanomaterial-based electrochemical biosensors: An overview," *Nanoscale*, vol. 7, no. 15, pp. 6420–6431, 2015, doi: 10.1039/c5nr00585j.
- [3] N. I. B. A. Shukri *et al.*, "Fabrication of Graphene Electrode via Graphene Transfer Method for Bisphenol A (BPA) Detection," *2021 IEEE Int. Conf. Sensors Nanotechnology, SENNANO 2021*, pp. 41–44, 2021, doi: 10.1109/SENNANO51750.2021.9642581.
- [4] V. Naresh and N. Lee, "A review on biosensors and recent development of nanostructured materials-enabled biosensors," *Sensors (Switzerland)*, vol. 21, no. 4, pp. 1–35, 2021, doi: 10.3390/s21041109.
- [5] A. D. Keefe, S. Pai, and A. Ellington, "Aptamers as therapeutics," *Nat. Rev. Drug Discov.*, vol. 9, no. 7, pp. 537–550, 2010, doi: 10.1038/nrd3141.
- [6] B. Kudłak and M. Wiczerzak, "Aptamer based tools for environmental and therapeutic monitoring: A review of developments, applications, future perspectives," *Crit. Rev. Environ. Sci. Technol.*, vol. 50, no. 8, pp. 816–867, 2020, doi: 10.1080/10643389.2019.1634457.
- [7] S. Johnson *et al.*, "Surface-Immobilized Peptide Aptamers as Probe Molecules for Protein Detection," vol. 80, no. 4, pp. 978–983, 2008.
- [8] Y. Wang, Z. Li, and H. Yu, "Aptamer-Based Western Blot for Selective Protein Recognition," vol. 8, no. October, pp. 1–9, 2020, doi: 10.3389/fchem.2020.570528.
- [9] X. Ni, M. Castanares, A. Mukherjee, and S. E. Lupold, "Nucleic Acid Aptamers: Clinical Applications and Promising New Horizons," pp. 4206–4214, 2011.
- [10] Z. Mei *et al.*, "Ultrasensitive one-step rapid visual detection of bisphenol A in water samples by label-free aptasensor," *Biosens. Bioelectron.*, vol. 39, no. 1, pp. 26–30, 2013, doi: 10.1016/j.bios.2012.06.027.
- [11] Y. Li, X. Zhai, X. Liu, L. Wang, H. Liu, and H. Wang, "Electrochemical determination of bisphenol A at ordered mesoporous carbon modified nano-carbon ionic liquid paste electrode," *Talanta*, vol. 148, pp. 362–369, 2016, doi: 10.1016/j.talanta.2015.11.010.
- [12] Y. Wang *et al.*, "<ACS Nano 2011 Wang Y.pdf>," *ACS Nano*, no. 12, pp. 9927–9933, 2011.
- [13] J. Phiri, P. Gane, and T. C. Maloney, "General overview of graphene: Production, properties and application in polymer composites," *Mater. Sci. Eng. B Solid-State Mater. Adv. Technol.*, vol. 215, pp. 9–28, 2017, doi: 10.1016/j.mseb.2016.10.004.
- [14] E. P. Randviir, D. A. C. Brownson, J. P. Metters, R. O. Kadara, and C. E. Banks, "The fabrication, characterisation and electrochemical investigation of screen-printed graphene electrodes," *Phys. Chem. Chem. Phys.*, vol. 16, no. 10, pp. 4598–4611, 2014, doi: 10.1039/c3cp55435j.
- [15] C. Cheng, S. Li, A. Thomas, N. A. Kotov, and R. Haag, "Functional Graphene Nanomaterials Based Architectures: Biointeractions, Fabrications, and Emerging Biological Applications," doi: 10.1021/acs.chemrev.6b00520.
- [16] T. T. Tran and A. Mulchandani, "Carbon nanotubes and graphene nano field-effect transistor-based biosensors," *TrAC - Trends Anal. Chem.*, vol. 79, pp. 222–232, 2016, doi: 10.1016/j.trac.2015.12.002.
- [17] J. Plutnar, M. Pumera, and Z. Sofer, "The chemistry of CVD graphene," *J. Mater. Chem. C*, vol. 6, no. 23, pp. 6082–6101, 2018, doi: 10.1039/c8tc00463c.

- [18] D. A. C. Brownson, D. K. Kampouris, and C. E. Banks, *Graphene electrochemistry: Fundamental concepts through to prominent applications*, vol. 41, no. 21. 2012.
- [19] E. P. Randviir, D. A. C. Brownson, M. Gómez-Mingot, D. K. Kampouris, J. Iniesta, and C. E. Banks, "Electrochemistry of Q-Graphene," *Nanoscale*, vol. 4, no. 20, pp. 6470–6480, 2012, doi: 10.1039/c2nr31823g.
- [20] S. Ullah *et al.*, "Graphene transfer methods : A review," vol. 14, no. 11, pp. 3756–3772, 2021.
- [21] S. N. Sabki, S. H. Shamsuri, S. F. Fauzi, M. L. Chon-Ki, and N. Othman, "Graphene transfer process and optimization of graphene coverage," *EPJ Web Conf.*, vol. 162, pp. 1049–1052, 2017, doi: 10.1051/epjconf/201716201049.
- [22] S. Ullah *et al.*, "Graphene transfer methods: A review," *Nano Res.*, vol. 14, no. 11, pp. 3756–3772, 2021, doi: 10.1007/s12274-021-3345-8.
- [23] A. C. Ferrari and D. M. Basko, "Raman spectroscopy as a versatile tool for studying the properties of graphene," *Nature Nanotechnology*, vol. 8, no. 4. pp. 235–246, 2013, doi: 10.1038/nnano.2013.46.
- [24] Y. Zhang, L. Wang, D. Lu, X. Shi, C. Wang, and X. Duan, "Sensitive determination of bisphenol A base on arginine functionalized nanocomposite graphene film," *Electrochim. Acta*, vol. 80, pp. 77–83, 2012, doi: 10.1016/j.electacta.2012.06.117.
- [25] P. Kumar, A. K. Singh, S. Hussain, and K. N. Hui, "Graphene : Synthesis , Properties and Application in Transparent Electronic Devices Graphene : Synthesis , Properties and Application in Transparent Electronic Devices," no. September 2015, 2013, doi: 10.1166/rase.2013.1043.
- [26] J. Chen, J. Li, L. Xu, W. Hong, Y. Yang, and X. Chen, "The glass-transition temperature of supported PMMA thin films with hydrogen bond/plasmonic interface," *Polymers (Basel)*, vol. 11, no. 4, 2019, doi: 10.3390/polym11040601.
- [27] I. O. Faniyi *et al.*, "The comparative analyses of reduced graphene oxide (RGO) prepared via green, mild and chemical approaches," *SN Appl. Sci.*, vol. 1, no. 10, pp. 1–7, 2019, doi: 10.1007/s42452-019-1188-7.
- [28] S. J. Kim, "Towards industrial applications of graphene electrodes My IOPscience Towards industrial applications of graphene electrodes This article has been downloaded from IOPscience . Please scroll down to see the full text article . View the table of contents for," no. July 2015, 2012, doi: 10.1088/0031-8949/2012/T146/014024.
- [29] V. Țucureanu, A. Matei, and A. M. Avram, "FTIR Spectroscopy for Carbon Family Study," *Crit. Rev. Anal. Chem.*, vol. 46, no. 6, pp. 502–520, 2016, doi: 10.1080/10408347.2016.1157013.
- [30] CUBoulder, "IR Spectroscopy Tutorial: Amines," no. 1752, pp. 2–4, 2011, [Online]. Available: <http://orgchem.colorado.edu/hnadbksupport/spectrtutor/amines.html>.
- [31] B. C. Smith, "Organic Nitrogen Compounds III: Secondary and Tertiary Amines," *Spectrosc.*, vol. 34, no. 5, pp. 22–26, 2019.
- [32] C. Ibaú, M. K. Md Arshad, G. Subash C.B., M. Nuzaihan, M. F. M. Fathil, and P. Estrela, "Gold interdigitated triple-microelectrodes for label-free prognosticative aptasensing of prostate cancer biomarker in serum," *Biosens. Bioelectron.*, vol. 136, no. March, pp. 118–127, 2019, doi: 10.1016/j.bios.2019.04.048.
- [33] E. Dollekamp, P. Bampoulis, D. P. Faasen, H. J. W. Zandvliet, and E. S. Kooij, "Charge Induced Dynamics of Water in a Graphene-Mica Slit Pore," *Langmuir*, vol. 33, no. 43, pp. 11977–11985, 2017, doi: 10.1021/acs.langmuir.7b02759.
- [34] Z. Hsine, S. Bizid, I. Zahou, L. Ben Haj Hassen, H. Nasri, and R. Mlika, "A highly sensitive impedimetric sensor based on iron (III) porphyrin and thermally reduced graphene oxide for detection of Bisphenol A," *Synth. Met.*, vol. 244, no. May, pp. 27–35, 2018, doi: 10.1016/j.synthmet.2018.06.014.
- [35] K. S. Kim, J. ryang Jang, W. S. Choe, and P. J. Yoo, "Electrochemical detection of Bisphenol A with high sensitivity and selectivity using recombinant protein-immobilized graphene electrodes," *Biosens. Bioelectron.*, vol. 71, pp. 214–221, 2015, doi: 10.1016/j.bios.2015.04.042.

